Progress in Quantum Electronics 85 (2022) 100417

Contents lists available at ScienceDirect

Progress in Quantum Electronics

journal homepage: www.elsevier.com/locate/pqe

Polarization anisotropy in nanowires: Fundamental concepts and progress towards terahertz-band polarization devices

Michael B. Johnston [a,*], Hannah J. Joyce [b,**]

[a] Department of Physics, University of Oxford, Clarendon Laboratory, Parks Rd, Oxford, OX1 3PU, United Kingdom
[b] Department of Engineering, University of Cambridge, Electrical Engineering, 9 JJ Thomson Ave, Cambridge, CB3 0FA, United Kingdom

ARTICLE INFO

Keywords:
Nanowire
Polarization
Anisotropy
Terahertz
Polarizer

ABSTRACT

Pronounced polarization anisotropy in semiconductor nanowires has been exploited to achieve polarization-sensitive devices operating across the electromagnetic spectrum, from the ultraviolet to the terahertz band. This contribution describes the physical origins of optical and electrical anisotropy in nanowires. Polarization anisotropy arising from dielectric contrast, and the behaviour of (nano)wire grid polarizers, are derived from first principles. This review discusses experimental observations of polarization-sensitive light–matter interactions in nanowires. It then describes how these phenomena are employed in devices that detect or modulate polarized terahertz radiation on ultrafast timescales. Such novel terahertz device concepts are expected to find use in a wide variety of applications including high-speed terahertz-band communications and molecular fingerprinting.

1. Introduction

Semiconductor nanowires are characterized by their linear, or quasi one-dimensional, geometry. This anisotropic geometry, combined with the nature of the nanoscale semiconductor itself, confers on nanowires some unique physical properties. One such property is strong optical and electrical polarization anisotropy, which arises in nanowires owing to a number of discrete effects, including dielectric contrast with the environment [1–5], selection rules in novel crystalline polytypes [6–8], and quantum confinement [9,10]. Absorption and emission coefficients therefore vary depending on whether the light is polarized parallel or perpendicular to the nanowire axis. Consequently, experimental measurements of photoluminescence (PL) [1,4], photoluminescence excitation (PLE) [5,8], photoconductivity [1,11,12], electroluminescence [13,14] and Raman scattering [15–19] show strong dependence on the polarization of the incident or emitted light relative to the nanowire axis.

This review will elucidate the physical mechanisms underlying polarization anisotropy in nanowires. The effect of dielectric contrast on polarization anisotropy will be derived from first principles by analytical solution of Maxwell's equations. This dielectric polarizability is the most common cause of polarization anisotropy, and is so pronounced that it is routinely used to align nanowires using dielectrophoresis [20] and to control the alignment of nanowires trapped with optical tweezers [21]. Dielectric contrast explains observations of polarization-dependent PL [22], terahertz (THz) absorption [11] and THz emission [23] in studies of semiconductor

Abbreviations: PL, photoluminescence; THz, terahertz; PLE, photoluminescence excitation; THz-TDS, terahertz time-domain spectroscopy; FDTD, finite-difference time-domain.

* Corresponding author.
** Corresponding author.
E-mail addresses: michael.johnston@physics.ox.ac.uk (M.B. Johnston), hannah.joyce@eng.cam.ac.uk (H.J. Joyce).

https://doi.org/10.1016/j.pquantelec.2022.100417

Available online 6 September 2022

nanowires.

We then discuss the implementation of nanowire-based polarization-sensitive THz devices. These are devices that operate in the THz band, lying between the microwave and infrared regions of the electomagnetic spectrum, and spanning approximately 0.1 THz to 10 THz [24]. Polarization-sensitive THz devices, such as receivers and polarizers, are the subject of increasing interest because a wealth of information can be transmitted in the full polarization state of THz light [25]. The ability to encode information in the polarization state of a THz carrier wave opens the door to polarization-division multiplexed and polarization modulated (polarization-shift keying) communication systems operating in the as-yet unallocated THz-band region of the electromagnetic spectrum [26,27]. In THz spectroscopy, the polarization state of THz light can reveal information about the anisotropic dielectric properties of the sample under investigation, such as the symmetry of molecular/lattice vibrations or quasiparticle excitations, or the orientation of the substructures (e.g. molecules or nanostructures) within a sample [28]. Extensions to THz time-domain spectroscopy (THz-TDS) such as THz Hall effect measurements [29,30], THz ellipsometry [31], THz cyclotron resonance [32] and THz tomography [33], all require THz polarimetry. To this end, efforts have focussed on developing THz polarizers, polarization modulators, and polarization-sensitive receivers.

The pronounced polarization anisotropy of semiconductor nanowires makes them ideal building blocks for THz polarization devices. Additionally, nanowire devices are miniature and easily integrated into existing systems, such as THz-TDS systems. After describing the fundamental origins and experimental observations of polarization anisotropy in nanowires, this review will examine the design, fabrication and operation of two types of nanowire-based THz polarization devices. Firstly, we discuss THz polarization modulators based on arrays of GaAs nanowires, which exhibit ultrafast modulation speeds ($<$ 10 ps) [11]. Secondly, we describe a photoconductive antenna based on crossed InP nanowires which has been demonstrated as an ultrafast detector capable of recording two orthogonal components of the THz electric field simultaneously [34].

2. Observations and origins of nanowire polarization anisotropy

Ruda and Shik [3] identified three mechanisms responsible for the polarization-dependence of optical absorption and emission in nanowires:

1. Dielectric contrast between the nanowire and its environment, leading to the classical phenomenon of dielectric confinement of the electric field,
2. Quantum confinement of carriers, leading to changes in energy levels of electronic states and the associated optical matrix elements, and
3. Modification of excitonic parameters owing to dielectric mismatch.

An additional mechanism that has come to light since their publication is

4. Appearance of wurtzite crystal phases, leading to changes in the bandstructure and the associated optical matrix elements.

These mechanisms are not mutually exclusive, and their superposition can also cause the observed optical anisotropy in nanowires. Mechanisms 2 and 3 must be considered for ultra-thin quantum wires where quantum confinement is significant, but can usually be disregarded for free-standing nanowires which tend to feature larger diameters.

2.1. Mechanism 1 - Dielectric contrast

Many experimental observations of polarization anisotropy are attributable to the dielectric contrast between the nanowire and its environment [1,2,4,5]. Semiconductor and metallic nanowires tend to have significantly higher dielectric constants than the surrounding environment (often air). If the nanowire is approximated as an infinitely long cylinder placed in a static electric field, solution of Maxwell's equations reveals that electric field components parallel to the nanowire axis will penetrate the nanowire unattenuated ($E_{\parallel}^{\text{in}} = E_{\parallel}^{\text{out}}$), whereas the penetration of electric field components perpendicular to the nanowire axis is suppressed by a factor

$$\frac{E_{\perp}^{\text{in}}}{E_{\perp}^{\text{out}}} = \frac{2\varepsilon_0}{\varepsilon_0 + \varepsilon_{\text{nw}}}, \tag{1}$$

where ε_0 is the dielectric constant of the environment and ε_{nw} is the dielectric constant of the nanowire. Section 3 will discuss the mathematical derivation of Equation (1) based on solution of Maxwell's equations. In the case of oscillating (non-static) electric fields such as terahertz, microwave, infrared, and visible radiation, Equation (1) is a valid approximation for the suppression of perpendicular electric field components within a nanowire, provided $a \ll \lambda$, where a is the nanowire radius and λ is the wavelength of the electromagnetic radiation [2].

The suppressed penetration of light polarized perpendicular to the nanowire axis has significant implications for the photoexcitation of nanowires. Specifically, illumination with a perpendicularly polarized laser will photoexcite fewer charge carriers than a parallel-polarized laser of the same incident intensity. This mechanism was responsible for observations of polarization-dependent PL in studies of single InP nanowires by Wang et al. [1]. Fig. 1a and Fig. 1b illustrate PL images acquired when InP nanowires were photoexcited with light polarized parallel or perpendicular, respectively, to the nanowire axis. Strong PL emission was observed when

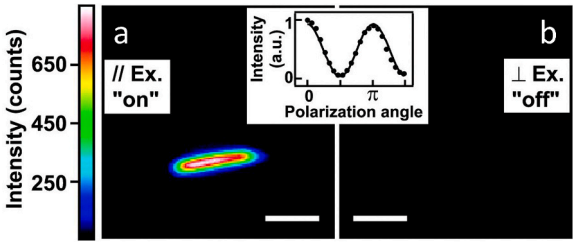

Fig. 1. PL images from a single zinc blende InP nanowire with excitation laser polarized (a) parallel and (b) perpendicular to the nanowire axis. Scale bars are 5 μm. Integrated PL emission intensity follows a $\cos^2$ dependence on the polarization angle relative to the nanowire axis (inset). Reproduced with permission from Wang et al. [1].

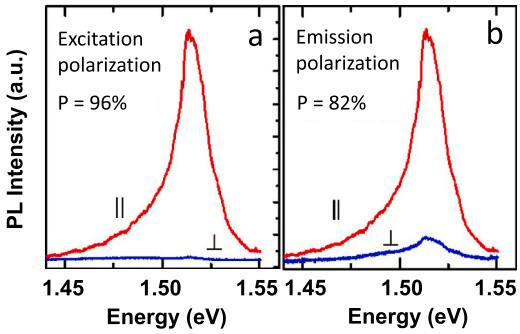

Fig. 2. PL spectra from a zinc blende GaAs/AlGaAs core–shell nanowire. (a) PL spectra measured with excitation laser polarized parallel (red) and perpendicular (blue) to the nanowire axis. (b) Polarization-resolved PL emission analyzed parallel (red) and perpendicular (blue) to the nanowire axis. For the spectra in (b), the excitation was polarized parallel to the nanowire axis. Reproduced with permission from Titova et al. [4].

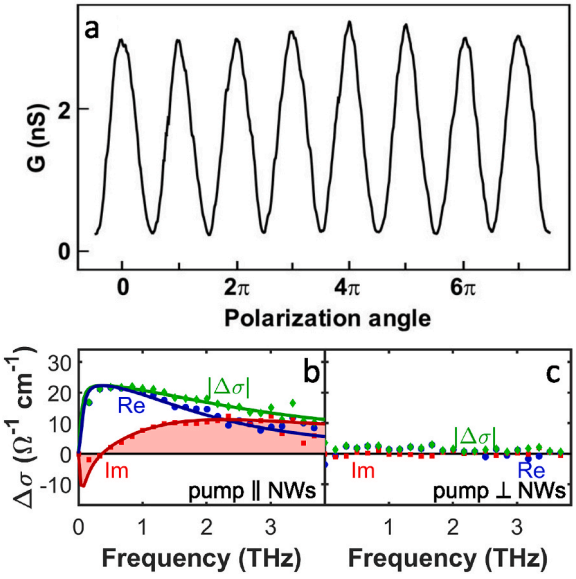

Fig. 3. Polarization-dependent photoconductivity of zinc blende III–V nanowires. (a) Photoconductance of InP nanowires measured between source and drain contacts as a function of polarization angle of the excitation laser relative to the nanowire axis. Reproduced with permission from Wang et al. [1]. (b, c) THz photoconductivity spectra of GaAs nanowires obtained 1 ps after photoexcitation with the excitation laser polarized (b) parallel and (c) perpendicular to the nanowire axis. The real part (blue), imaginary part (red) and magnitude (green) of the complex conductivity are plotted. The solid lines are a Drude–Lorentz fit to the data. Reproduced with permission from Baig et al. [11]. Copyright 2017 American Chemical Society.

the excitation was polarized parallel to the nanowire axis (Fig. 1a) but was absent when the excitation was polarized perpendicular to the nanowire (Fig. 1b). The integrated PL emission follows a $\cos^2$ dependence on the polarization angle of the incident light relative to the nanowire axis, as shown in the inset of Fig. 1. Similar effects were observed in GaAs/AlGaAs core–shell nanowires [4] as demonstrated in the PL spectra of Fig. 2a for excitation light polarized parallel and perpendicular to the long-axis of a single nanowire. The degree of excitation polarization, $P = 96\%$, is calculated as $P = \frac{I_{\parallel} - I_{\perp}}{I_{\parallel} + I_{\perp}}$ where $I_{\parallel}$ and $I_{\perp}$ are the PL intensities after photoexcitation with light polarized parallel and perpendicular to the nanowire respectively.

In addition, for both InP [1] and GaAs/AlGaAs nanowires [4], the emitted PL was strongly polarized parallel to the nanowire axis. This is exemplified in the spectra of Fig. 2b taken from a single GaAs/AlGaAs core–shell nanowire. Ruda and Shik [2] studied the origin of polarized light emission from nanowires by considering the orientation and strength of the electric dipole moments giving rise to light emission, under the standard assumptions of a static electric field and cylindrical nanowire geometry. They calculated that, for the case of dipoles oriented perpendicular to the nanowire axis, dielectric contrast reduces the effective dipole moment by $\frac{2\varepsilon_0}{\varepsilon_0 + \varepsilon_{nw}}$ compared to the dipole moment for dipoles oriented parallel to the nanowire axis [2]. The greater oscillator strength of the parallel dipoles contributes to the strong PL emission polarized parallel to the nanowire axis, as is indeed observed experimentally.

This mechanism for polarized PL emission is independent of the polarization of the original excitation laser. If, however, polarized excitation has induced a non-equilibrium distribution of dipole orientations, the PL emission polarization can retain a memory of the original excitation laser's polarization. Hoang et al. investigated such an effect in their polarization-resolved PLE spectroscopy study of exciton spin scattering in GaAs/AlGaAs core–shell nanowires [5]. In their study, the PL emission polarization was particularly influenced by the excitation polarization when the excitation energy was resonant with the optical transitions of excitons together with longitudinal optical phonons. The interpretation of this result was that resonant excitation with a linearly polarized laser produced a non-equilibrium population of exciton spin states. After resonant excitation, the polarization of PL emission was a function of this distribution of exciton spins coupled with the dielectric contrast. In contrast, after non-resonant excitation with higher energy photons, spin-scattering processes depolarize the exciton spin distributions, reducing the influence of the original excitation polarization.

Dielectric contrast is also responsible for observations of polarization-dependent photoconductivity. Fig. 3a illustrates the variation in conductance of an electrically-contacted InP nanowire as the photoexcitation laser's polarization is varied from 0° (parallel) to 90° ($\frac{\pi}{2}$, perpendicular) and beyond. Minima in conductance are observed whenever the excitation laser is polarized perpendicular to the nanowire axis, as anticipated given the suppression of electric field within the nanowire for perpendicular electric field components. Similar effects are seen in the THz photoconductivity spectra of GaAs nanowires in Fig. 3b and c. Here, the photoconductivity ($\Delta\sigma$) is entirely suppressed when the excitation pulse is polarized perpendicular to the nanowire axis (Fig. 3c). This phenomenon underpins the operating principle of the ultrafast THz polarization modulator described in Section 4.2.

2.2. Mechanism 2 - Quantum confinement

In ultra-thin quantum wires (radii < 10 nm), charge carriers experience quantum confinement in the radial direction. This affects the optical matrix elements, such that some transitions are suppressed for particular polarizations of light relative to the direction of confinement [9,10,35]. This effect was observed in PLE spectroscopy of GaAs quantum wires, which showed that the lowest energy conduction band-to-valence band transition is excited by light polarized parallel to the wire axis whereas the next lowest transition is excited by light polarized perpendicular to the wire axis [36].

Although quantum confinement is significant in ultra-thin quantum wires, it does not play a significant role in the optical behaviour of free-standing nanowires whose radii are typically more than a few tens of nanometers [3]. This is because as the nanowire radius increases, the quantization energy decreases, eventually dropping below the thermal energy or below the energetic broadening of the quantized energy levels.

2.3. Mechanism 3 - Dielectrically enhanced excitons

This effect, which can be considered a combination of Mechanisms 1 and 2, has been observed in ultra-thin GaAs, InP and CdSe quantum wires of radii < 10 nm [37]. The dielectric contrast between the quantum wire and its surroundings modifies the exciton binding energies and oscillator strengths to yield marked polarization anisotropy. This effect can be usually be disregarded for free-standing nanowires, as their radii tend to be larger than the Bohr exciton radius in the nanowire material (e.g. 13 nm in GaAs).

2.4. Mechanism 4 - Wurtzite crystal phases

Polarization anisotropy can arise owing to optical selection rules imposed by the nanowire bandstructure [38]. III–V nanowires can famously exhibit the hexagonal wurtzite crystal phase (C_{6v} point-group) instead of the standard cubic zinc blende crystal phase (T_d point-group) that is thermodynamically stable for bulk III–Vs (with the exception of nitrides). Both the wurtzite structure and the zinc blende phase have been achieved in GaAs, InAs, GaP and InP nanowires [39], and these phases are accompanied by distinct band-structures [40].

In bulk zinc blende materials, optical transitions between the valence band and conduction band are allowed for any polarization of light. On the other hand, in wurtzite materials, the wavefunctions of certain electronic states in the various valence and conduction bands have symmetries that only permit band-to-band transitions involving excitation or emission of light polarized perpendicular to the c-axis ([0001] crystallographic direction) [6,7]. As wurtzite nanowires exclusively grow along the c-axis, this means that such

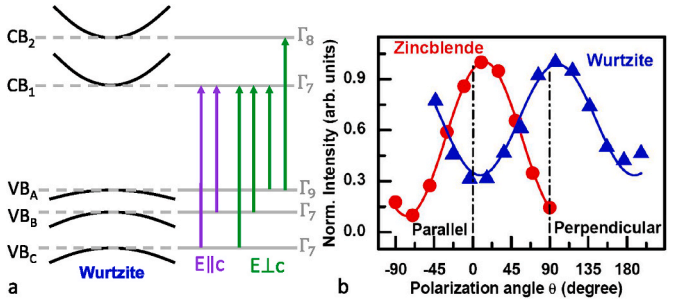

Fig. 4. (a) Band diagram illustrating allowed optical transitions between three valence bands (VB_A, VB_B, and VB_C) and two conduction bands (CB_1 and CB_2) in wurtzite crystals for light polarized parallel and perpendicular to the nanowire axis. The lowest energy transition ($\Gamma_9 \rightarrow \Gamma_7$) is only allowed for light polarized perpendicular to the nanowire axis. (b) Polarization-resolved PL emitted from zinc blende and wurtzite InP nanowires. The angle θ is the polarization angle of the emitted PL relative to the nanowire axis. The solid line is a $\cos^2\theta$ fit to the data. Panel (b) is reproduced with permission from Mishra et al. [8].

optical transitions are only permitted for light polarized perpendicular to the nanowire axis. Specifically, transitions from the highest lying Γ_9 symmetry valence band to the two lowest lying Γ_7 and Γ_8 conduction bands are polarized perpendicular to the c-axis. Fig. 4a illustrates the optical selection rules for transitions between the valence bands and conduction bands for light polarized parallel and perpendicular to the nanowire c-axis. These selection rules manifest as polarized PL emission from wurtzite InP and GaAs nanowires [8,41,42], and polarization-sensitive photoconductivity in wurtzite InAs nanowires [12]. Fig. 4b compares the polarization of PL emission from zinc blende and wurtzite nanowires. The PL emitted from the zinc blende nanowire follows a $\cos^2$ dependence on polarization angle relative to the nanowire axis, as explained by Mechanism 1 (Section 2.1). In marked contrast, the PL emitted from the wurtzite InP nanowire is strongly polarized perpendicular to the nanowire axis, owing to the optical selection rules for band-edge transitions. The degree of polarization anisotropy for the wurzite nanowire is not so pronounced as for the zinc blende nanowire because Mechanism 1 also affects the wurtzite nanowire, which somewhat counteracts the effect of the selection rules.

3. Mathematical derivation of polarization-dependent electric field within a nanowire

The strong polarization anisotropy of nanowires to electromagnetic radiation can be modelled with high accuracy by numerical methods such as solving Maxwell's equations with finite-difference time-domain (FDTD) [43–46] or scattering matrix [47] methods. However, arguably more physical insight may be obtained by applying simple electrostatics and sensible approximations to such problems. In that case, simple analytical expressions can be obtained for quantities such as the anisotropy of absorption of both optical and THz photons by nanowires. Here we derive an expression for how the electric field inside a nanowire is related to an externally applied static electric field. To obtain a simple analytic expression we made a few assumptions: (1) we ignore crystalline facets of the nanowire and treat it as a dielectric cylinder of radius a, and (2) we approximate the nanowire as a cylinder of infinite length. The justification of this last approximation is the large aspect ratio of typical nanowires, which may be tens of microns in length, yet only 10–100 nm in radius.

The analysis presented in Sections 3.1 and 3.2 invokes electrostatics by solving Gauß's law $\nabla\mathbf{E} = \frac{\rho}{\varepsilon}$ for the two limiting cases of a (i) dielectric cylinder and a (ii) metallic cylinder, respectively. The first case is relevant to the polarization anisotropy of optical absoprtion in nanowires and the second case to THz absorption anisotropy.

3.1. Case of a dielectric nanowire

Consider the case of a non-conductive, purely dielectric nanowire. We assume the cylinder is a pure dielectric of (real) dielectric constant $\varepsilon_{\mathrm{nw}}$ without free charge (i.e. a non-photoexcited undoped nanowire). In that case we can use Gauß's law with the enclosed charge density being zero ($\rho = 0$), i.e. $\nabla\mathbf{E} = 0$. Combining this with $\mathbf{E} = -\nabla\varphi$, gives Laplace's equation $\nabla^2\varphi = 0$ which with appropriate boundary conditions may be solved to find the electric potential φ inside and outside of the nanowire. The Laplace equation in cylindrical coordinates is

$$\frac{1}{r}\frac{\partial}{\partial r}\left(r\frac{\partial\varphi}{\partial r}\right) + \frac{1}{r^2}\frac{\partial^2\varphi}{\partial\theta^2} + \frac{\partial^2\varphi}{\partial z^2} = 0. \tag{2}$$

We set the coordinate system so the nanowire axis is coincident with the z-axis, and assume a constant external electric field E_0 is applied in the x-direction. Since we assume the nanowire has infinite length, by symmetry there can be no z-dependence in φ, thus we can ignore the last term. This equation can now be solved by the separation of variables technique:

Substituting $\varphi(r, \theta) = Y(r)S(\theta)$ into Equation (2) gives

$$\frac{r}{Y}\frac{\mathrm{d}}{\mathrm{d}r}\left(r\frac{\mathrm{d}Y}{\mathrm{d}r}\right) = -\frac{1}{S}\frac{\mathrm{d}^2S}{\mathrm{d}\theta^2} = k \tag{3}$$

where k is a constant as the term in r is independent of the term in θ. The solution of

$$-\frac{1}{S}\frac{\mathrm{d}^2 S}{\mathrm{d}\theta^2} = k \tag{4}$$

gives $S(\theta)$ as a linear superposition of terms in the form $\cos(k^{\frac{1}{2}}\theta)$ and $\sin(k^{\frac{1}{2}}\theta)$ but the solutions are restricted to single-valued functions of θ, that is

$$\begin{aligned} \cos k^{\frac{1}{2}}(\theta + 2\pi) &= \cos k^{\frac{1}{2}}\theta \\ \sin k^{\frac{1}{2}}(\theta + 2\pi) &= \sin k^{\frac{1}{2}}\theta, \end{aligned} \tag{5}$$

which is only possible if $k = n^2$ where $n \in \mathbb{Z}$. We can also require $n \geq 0$ without loss of solutions.

Likewise the solution of

$$\frac{r}{Y}\frac{\mathrm{d}}{\mathrm{d}r}\left(r\frac{\mathrm{d}Y}{\mathrm{d}r}\right) = k \tag{6}$$

gives $Y(r)$ in the form $r^{\pm n}$ for $n \in \mathbb{N}$ and $\ln r$ + constant for $n = 0$. Therefore the solution of the Laplace equation with no z-dependence, $\varphi(r, \theta)$, is a linear superposition

$$\begin{aligned} \varphi(r,\theta) &= Y(r)S(\theta) \\ &= A + B\ln(r) + \sum_n (C_n r^n \cos(n\theta) + D_n r^{-n}\cos(n\theta) + E_n r^n \sin(n\theta) + F_n r^{-n}\sin(n\theta)\,). \end{aligned} \tag{7}$$

The uniform external electric field $\mathbf{E}_0 = E_0\mathbf{i}$ is applied in the x-direction with the nanowire axis in the z-direction, so the potential must be symmetric in y (i.e. there is mirror symmetry in the $x - z$ plane). This implies that $\varphi(\theta) = \varphi(-\theta)$, thus for this particular problem all sin $n\theta$ terms must be zero (i.e. $E_n = F_n = 0\ \forall n$). In addition the ln r term must vanish in the case that the nanowire is not charged, as it diverges at $r = 0$ inside the nanowire ($[\ln r]_{\lim\, r\to 0} \to -\infty$) and does not converge at a large distance from the nanowire ($[\ln r]_{\lim\, r\to\infty} \to \infty$).

Firstly consider the potential outside the nanowire. At large distances the external field should not be distorted significantly so $[E(r,\theta)]_{r\to\infty} = E_0\mathbf{i}$. This means that any term of r^n with $n > 1$ must be zero (i.e. $C_n = 0\ \forall n > 1$). Since $\mathbf{E} = -\nabla\varphi$,

$$\begin{aligned} [\varphi(r,\theta)]_{r\to\infty} &= -E_0 x + \text{constant} \\ &= -E_0 r\cos\theta + \text{constant}. \end{aligned} \tag{8}$$

Comparing Equation (7) with Equation (8) implies that $C_1 = -E_0$ outside the nanowire cylinder (i.e. $r > a$). Thus the potential outside the cylinder is

$$\varphi^{\text{out}}(r,\theta) = A^{\text{out}} - E_0 r\cos\theta + \sum_{n=1}^{\infty}\frac{D_n^{\text{out}}}{r^n}\cos n\theta \qquad \text{for} \quad r > a\,. \tag{9}$$

Now consider the form of the potential inside the nanowire. As we have assumed the nanowire is uncharged there should be no singularities, so φ must remain finite as $r \to 0$. This means that any term of r^{-n} with $n \geq 1$ must be zero (i.e. $D_n = 0\ \forall n$). So the potential inside the cylinder is

$$\varphi^{\text{in}}(r,\theta) = A^{\text{in}} + \sum_{n=1}^{\infty} C_n^{\text{in}} r^n \cos n\theta \qquad \text{for} \quad r \leq a. \tag{10}$$

However both these equations must obey two boundary conditions at the surface of the nanowire:

1. The tangential component of $\mathbf{E}$ must be continuous across the interface (curl $\mathbf{E} = 0$), hence

$$\varphi^{\text{out}}(a,\theta) = \varphi^{\text{in}}(a,\theta) \tag{11}$$

2. The radial component of electric displacement $\mathbf{D}$ must be continuous at the interface

$$D_r^{\text{out}}(a,\theta) = D_r^{\text{in}}(a,\theta) \tag{12}$$

where

$$D_r = -\varepsilon\frac{\partial\varphi}{\partial r}, \tag{13}$$

is the radial component of electric displacement in cylindrical coordinates and ε is the dielectric constant.

As all members of the set $\{\cos n\theta\}(n = 0, 1, 2, \ldots)$ are orthogonal on the interval $[0, 2\pi]$, we can treat each cos $n\theta$ term in Equations (9) and (10) separately when applying the two boundary conditions Equation (11) and Equation (12). We can now determine each of

the unknown coefficients in Equation (9) and Equation (10) by considering each value of n:

- $n = 0$: Equation (11) implies that $A^{\text{out}} = A^{\text{in}}$.
- $n = 1$: Subsituting the $n = 1$ terms of Equation (9) and Equation (10) into the first boundary condition Equation (11) gives

$$\begin{aligned} \varphi^{\text{out}}(a,\theta) &= \varphi^{\text{in}}(a,\theta) \\ -E_0 a + D_1^{\text{out}} a^{-1} &= C_1^{\text{in}} a \end{aligned} \tag{14}$$

and now into the second boundary condition Equation (12),

$$\begin{aligned} D_r^{\text{out}}(a,\theta) &= D_r^{\text{in}}(a,\theta) \\ \left[-\varepsilon^{\text{out}}\frac{\partial\varphi^{\text{out}}}{\partial r}\right]_{r=a} &= \left[-\varepsilon^{\text{in}}\frac{\partial\varphi^{\text{in}}}{\partial r}\right]_{r=a} \\ \varepsilon^{\text{out}}\left(E_0 + D_1^{\text{out}}a^{-2}\right)\cos\theta &= -\varepsilon^{\text{in}}C_1^{\text{in}}\cos\theta \\ E_0 + \frac{D_1^{\text{out}}}{a^2} &= -\frac{\varepsilon^{\text{in}}}{\varepsilon^{\text{out}}}C_1^{\text{in}}. \end{aligned} \tag{15}$$

Combining Equations (14) and (15) gives:

$$C_1^{\text{in}} = \frac{-2E_0}{1+K}, \tag{16}$$

where we define $K = \varepsilon^{\text{in}}/\varepsilon^{\text{out}}$. Now substituting C_1 back into Equation (14) gives

$$D_1^{\text{out}} = E_0 a^2 \frac{K-1}{K+1}. \tag{17}$$

- $n \geq 2$: The first boundary condition Equation (11) gives

$$\begin{aligned} D_n^{\text{out}} a^{-n} &= C_n^{\text{in}} a^n \\ D_n^{\text{out}} &= C_n^{\text{in}} a^{2n} \end{aligned} \tag{18}$$

and the second boundary condition Equation (12) gives,

$$\begin{aligned} \varepsilon^{\text{out}} D_n^{\text{out}} n a^{-(n+1)} &= -\varepsilon^{\text{in}} C_n^{\text{in}} n a^{(n-1)} \\ D_n^{\text{out}} &= -\frac{\varepsilon^{\text{in}}}{\varepsilon^{\text{out}}} C_1^{\text{in}} a^{2n}. \end{aligned} \tag{19}$$

Combining Equations (18) and (19) to eliminate D_n^{out} gives

$$C_n^{\text{in}} a^{2n}\left(1 + \frac{\varepsilon^{\text{in}}}{\varepsilon^{\text{out}}}\right) = 0 \tag{20}$$

so

$$C_n^{\text{in}} = 0 \quad \forall n \geq 2. \tag{21}$$

Now substituting $C_n^{\text{in}} = 0$ back into Equation (18) gives

$$D_n^{\text{out}} = 0 \quad \forall n \geq 2. \tag{22}$$

Substituting these values back into Equations (9) and (10) gives the electric potential in terms of the applied external electric field E_0 as

$$\varphi(r,\theta) = \begin{cases} \varphi^{\text{in}} = -\dfrac{2}{1+K} r E_0 \cos\theta & r \leq a \quad \text{inside} \\ \varphi^{\text{out}} = \left(\dfrac{a^2}{r}\dfrac{K-1}{K+1} - r\right) E_0 \cos\theta & r > a \quad \text{outside} \end{cases} \tag{23}$$

where we have set $A^{\text{out}} = A^{\text{in}} = 0$ since the offset of a potential is arbitrary.

Therefore the electric field is just

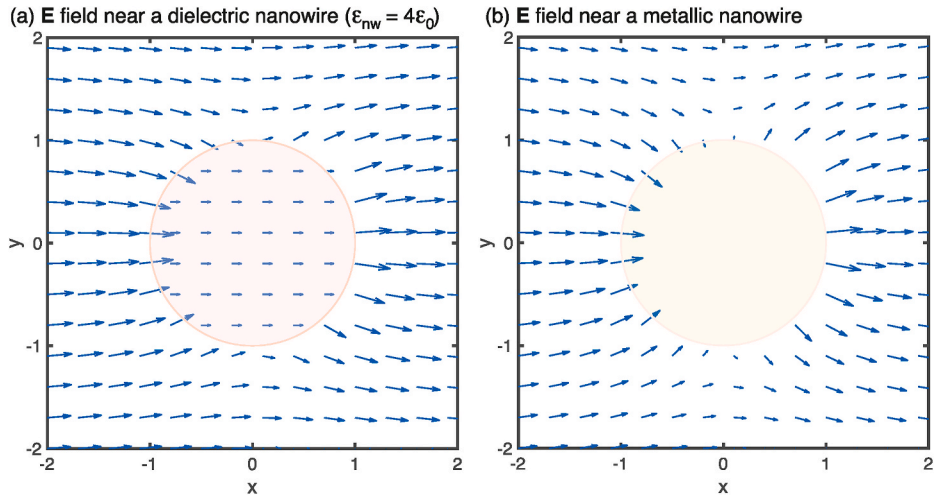

Fig. 5. Electric vector field in the vicinity of a nanowire in a constant external electric field. Two cases are shown, a cross-section through (a) a dielectric nanowire with a relative dielectric constant of 4 ($\varepsilon_{nw} = 4\varepsilon_0$) and (b) a metallic nanowire. The arrows represent the electric field at the position of the tail of the arrow. The figures are generated according to Equations (25) and (29) respectively. The pink and gold shaded regions represent cross-sections through the dielectric and metallic nanowires respectively. The radii of the nanowires are set to $a = 1$ arbitrary unit, but as we are dealing with a DC electric field the problem is scalable. Note that the dielectric constant of 4 is chosen so that the electric field vectors inside the dielectric nanowire can be seen clearly on the plot. For most semiconducting nanowires the dielectric constant would be much higher (~ 12) making the arrows too hard to visualise.

$$\begin{aligned}\mathbf{E}^{\text{in}} &= -\nabla\,\varphi^{\text{in}}(r,\theta)\\ &= -\left(\frac{\partial\varphi^{\text{in}}}{\partial r}\widehat{\mathbf{r}} + \frac{1}{r}\frac{\partial\varphi^{\text{in}}}{\partial\theta}\widehat{\boldsymbol{\theta}}\right)\end{aligned} \tag{24}$$

so the electric field inside and outside the nanowire is

$$\mathbf{E}(r,\theta) = \begin{cases} \mathbf{E}^{\text{in}} = \dfrac{2E_0}{1+K}(\cos\theta\widehat{\mathbf{r}} - \sin\theta\widehat{\boldsymbol{\theta}}) & r \le a \ \text{ inside} \\ \mathbf{E}^{\text{out}} = E_0\left[\left(\dfrac{a^2}{r^2}\dfrac{K-1}{K+1}+1\right)\cos\theta\widehat{\mathbf{r}} + \left(\dfrac{a^2}{r^2}\dfrac{K-1}{K+1}-1\right)\sin\theta\widehat{\boldsymbol{\theta}}\right] & r > a \ \text{ outside.}\end{cases} \tag{25}$$

In the case of a nanowire with dielectric constant ε_{nw} in a vacuum, $K = \varepsilon_{\text{nw}}/\varepsilon_0$ and noting that the r^{-2} terms in Equation (25) disappears as $r \to \infty$ it follows that

$$\mathbf{E}^{\text{in}} = \frac{2\varepsilon_0}{\varepsilon_0 + \varepsilon_{\text{nw}}}[\mathbf{E}^{\text{out}}]_{\lim\, r\to\infty}. \tag{26}$$

So if an external electric field of strength E_0 is applied in the x-direction (i.e. perpendicular to the long axis of the nanowire) the electric field inside the nanowire will also be in that direction, but will be reduced by a factor

$$\frac{2\varepsilon_0}{\varepsilon_0 + \varepsilon_{\text{nw}}}. \tag{27}$$

This is Equation (1) of Section 2.1 and is the expression that was used by Wang et al. [1] to explain why a nanowire absorbs light less well when the light is polarized orthogonal to the long axis of the nanowire. Of course light and THz waves are time-varying electromagnetic fields, whereas the analysis above assumed a static electric field. However it can be seen by simulating the interaction of electromagnetic waves with dielectric cylinders [45,46], using a FDTD approach, that the electric field enhancement is similar to our simple analytic model. In addition the FDTD simulations allow the faceted nature of real nanowires to be modelled to assess the impact of localized electric-field enhancement which is not considered in the analytic approach here owing to the approximation of nanowires as cylinders. With these provisos the analytic approach still provides an intuitive picture of general polarization anisotropy in nanowires.

Ruda and Shik [3] extended their analytical solution of Maxwell's equations to time-varying electromagnetic fields. This extension is necessary for large-diameter nanowires where the approximation $a \ll \lambda$ is no longer valid and light waves cannot be approximated as static electric fields. They uncovered a non-monotonic frequency dependence of electric field penetration into the nanowire for both parallel and perpendicular polarizations. Resonances of absorption and emission occurred at different frequencies for parallel and perpendicularly-polarized radiation. The calculations revealed that for large-diameter nanowires, certain resonant frequencies would experience enhanced absorption or emission of perpendicularly polarized light, in contrast to predictions and experimental

observations for smaller diameter nanowires described by Equation (1).

3.2. Case of a metallic nanowire

A semiconductor nanowire can be made electrically conductive by photoexcitation or doping. We can again gain physical insight and analytic solutions using simple electrostatics. Let's make the assumption that the conductive nanowire is a perfect metal. We know from Gauß's law that in this case there is no electric field inside the nanowire, because the free charge inside such a perfectly conductive nanowire can rearrange to screen any external electric field. Thus that our perfect metal nanowire is infinitely polarizable. In our model above this may be represented by $\varepsilon_{\mathrm{nw}} \to \infty$ which implies $K \to \infty$ in Equation (25) and gives the electric potential as

$$\varphi(r,\theta) = \begin{cases} \varphi^{\mathrm{in}} = 0 & r \le a \quad \text{inside} \\ \varphi^{\mathrm{out}} = \left(\dfrac{a^2}{r} - r\right) E_0 \cos(\theta) & r > a \quad \text{outside} \end{cases} \tag{28}$$

and

$$\mathbf{E}(r,\theta) = \begin{cases} 0 & r \le a \quad \text{inside} \\ E_0\left[\left(\dfrac{a^2}{r^2}+1\right)\cos\theta\hat{\mathbf{r}} + \left(\dfrac{a^2}{r^2}-1\right)\sin\theta\hat{\boldsymbol{\theta}}\right] & r > a \quad \text{outside.} \end{cases} \tag{29}$$

Note that the same result is achieved by replacing the boundary conditions, Equations (11) and (14), of the dielectric case in Section 3.1 with $\varphi_{\mathrm{out}}(a,\theta) = \varphi_0 = 0$ (i.e. the electric potential is constant at the surface of a conductor, and we are free to set that value to zero).

Fig. 5 illustrates the electric field vectors arising within dielectric and metallic nanowires placed in an external static electric field polarized perpendicular to the nanowire axis. These vectors were calculated using Equations (25) and (29).

4. Nanowire THz polarizers and modulators

The strong anisotropy of the static electric field distribution in the vicinity of nanowires, as indicated by Equations (25) and (29), suggests that nanowires have the potential to be components of polarizers for electromagnetic waves. Indeed arrays of aligned metallic carbon nanotubes have been demonstrated as excellent polarizers for THz radiation [48]. In 2014 non-aligned arrays of semiconducting carbon nanotubes were found to act as a polarizer when photoexcited with linearly polarized laser light, thus demonstrating the concepts of an optically switchable THz polarizer [49]. This study reported sub-picosecond switching and rotation of THz polarization, but the polarization modulation was very weak.

Arrays of aligned III-V semiconductor nanowires proved much more practical with a significantly improved modulation depth [11]. In addition, the ability to engineer radial heterostructures allows for fine control over surface recombination and hence device switching times [50,51]. In combination with a static wire grid polarizer this device becomes a fast amplitude modulator, but potentially more interesting is its ability to modulate and compose particular polarization states [23]. We will briefly consider the basic concept of a nanowire polarizer before calculating its expected performance with elementary analytic electromagnetism.

An array of aligned nanowires functions as a dynamic wire grid polarizer by controlling the conductivity of the nanowires via optical excitation. When such an array of nanowires is excited with above-bandgap light, electron–hole pairs are generated and the nanowires become conductive. If the photo-injected charge density is high enough that the plasma frequency of charge carriers in the nanowires is higher than the THz radiation frequency, then the nanowires appear metallic to the THz radiation. However when the light is switched off electrons and holes recombine and the plasma frequency of charges in the semiconductor will then fall below the frequency of the THz radiation and the nanowires appear to the THz radiation as a non-conductive dielectric effective medium with a very much weaker polarization anisotropy.

Static polarizers consisting of grids of metal wires have long been used as linear polarizers in the microwave, far-infrared, millimetre, sub-millimetre, THz and even mid-infrared parts of the electromagnetic spectrum [52,53]. The dynamic nanowire polarizer [11,49] is essentially an extension of the static polarizer concept, the extension being the ability to make the metal wires appear (via photoexcitation) and disappear (via recombination) to the THz radiation. Therefore an understanding of how electromagnetic waves interact with an array of aligned wires is very informative when designing both static and dynamic polarization devices.

4.1. Analytic treatment of a nanowire wire grid polarizer

Here we consider the case of how electromagnetic waves interact with a grid of metal wires. The aim is to create an intuitive picture of how wire grid polarizers work, and perform some elementary quantitative analysis. This problem has a long history, having been solved by Lord Rayleigh [54,55], JJ Thomson [56] and H Lamb [57]. While a thorough account can be found in these original references, we will outline the approach taken by McDonald [58] and discuss the validity of the assumptions and approximations for the case of semiconductor nanowires.

We now consider a periodic grid of metal nanowires of radius a. As before we choose our coordinate system such that the long axes of the nanowires are aligned along the z-direction. Nanowires are placed at intervals of length d along the y-axis at positions $y = nd$ as illustrated in Fig. 6. We assume that the nanowires have infinite length and that the nanowire radius a is much smaller than the

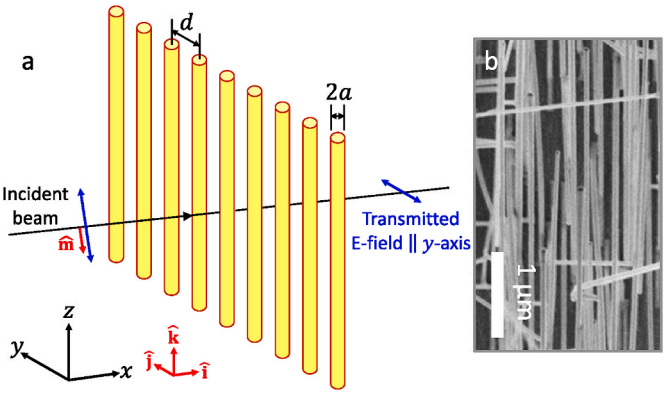

Fig. 6. (a) Schematic diagram illustrating the configuration of a wire grid polarizer. A beam of arbitrary polarization defined by unit vector $\hat{\mathbf{m}}$ is incident on the polarizer. The electric field component along the y-axis is transmitted. (b) Scanning electron micrograph of aligned GaAs nanowires with random spacings comprising a THz wire grid polarizer. Panel (b) is reproduced with permission from Baig et al. [11]. Copyright 2017 American Chemical Society.

wavelength of incident THz light. It is clear by comparing the nanowires we will model (Fig. 6a) with the way nanowires are aligned in a real-world device (Fig. 6b) that real nanowire devices are likely to utilize nanowires that are not perfectly aligned and not in a perfect regular array. However, to allow a simple analytic analysis we assume a perfectly aligned regular periodic array and ignore crystal facets on the walls of the NWs. Our aim here is to calculate the reflection and transmission of a plane wave of THz light travelling in the positive x-direction in vacuum.

The electric field of THz light, $\mathbf{E}(\mathbf{r}, t)$ must satisfy the wave equation

$$\left(\nabla^2 - \frac{1}{c^2}\frac{\partial^2}{\partial t^2}\right)\mathbf{E}(\mathbf{r}, t) = 0. \tag{30}$$

We will assume that $\mathbf{E}(\mathbf{r}, t)$ is polarized along a particular direction $\hat{\mathbf{m}}$ in the y–z plane so that $\mathbf{E}(\mathbf{r},t) = E(\mathbf{r},t)\hat{\mathbf{m}}$. We can now solve the wave equation using the method of separation of variables by substituting in $E(\mathbf{r}, t) = A(\mathbf{r})T(t)$ to give,

$$\frac{\nabla^2 A}{A} = \frac{1}{c^2 T}\frac{\partial^2 T}{\partial t^2} = -k^2 \tag{31}$$

where $-k^2$ is an arbitrary constant. Thus we have two separate equations,

$$\frac{\partial^2 T(t)}{\partial t^2} = -k^2 c^2 T(t) \tag{32}$$

which has the solution $T(t) = Ce^{-i\omega t}$ where $k = \omega/c$, and

$$(\nabla^2 + k^2)A(\mathbf{r}) = 0. \tag{33}$$

For this problem the infinite extent of the nanowires in the z-direction and the infinite extent of the incoming plane wavefront in the y–z plane implies that there should be no spatial variation of the THz electric field in the z-direction, $A(\mathbf{r}) = A(x, y)$. In addition as Equation (33) is separable in x and y we may write $A(\mathbf{r}) = A(x, y) = X(x)Y(y)$, while the periodicity of the nanowires in the y-directions means that it is helpful to write $Y(y)$ as a Fourier series of period d, that is,

$$Y(y) = \sum\nolimits_{n=0}^{\infty} C_n \cos\left(\frac{2\pi n y}{d}\right), \tag{34}$$

where $\{C_n\}$ are Fourier coefficients and n is a positive integer. This symmetry also suggests that the solution in the x direction is likely to be exponentially decaying, so we can trial the solution

$$A(x, y) = \sum_{n=0}^{\infty} C_n e^{k_n x}\cos\left(\frac{2\pi n y}{d}\right) \tag{35}$$

which by substitution into Equation (33) and equating Fourier terms allows us the determine k_n as

$$k_n = \begin{cases} \pm ik & \text{for} \quad n = 0 \\ \pm\sqrt{\left(\frac{2\pi n}{d}\right)^2 - k^2} & \text{for} \quad n > 0. \end{cases} \tag{36}$$

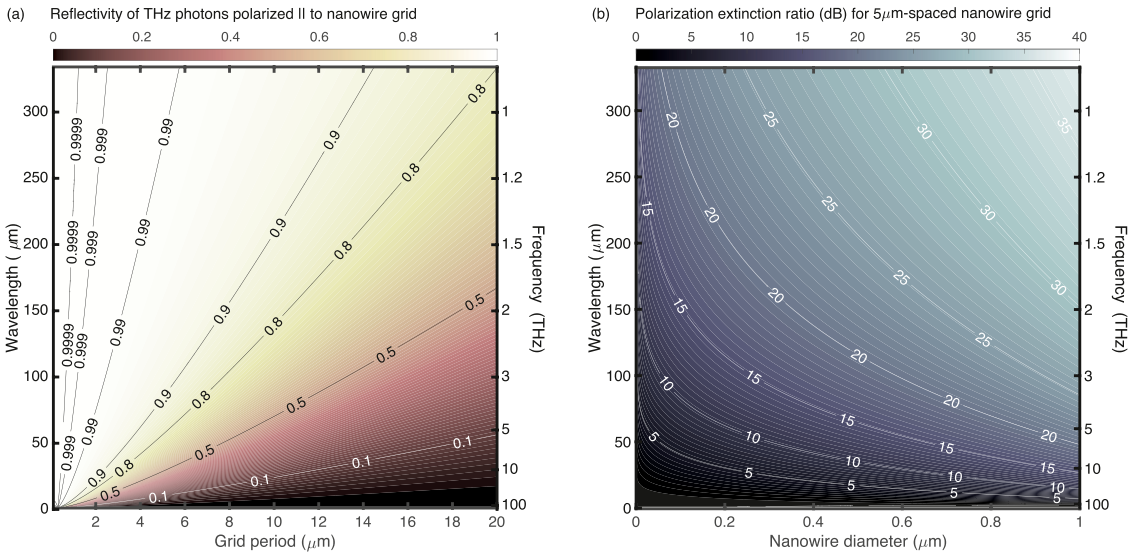

Fig. 7. (a) Reflectivity $R_\parallel$ of THz radiation from a grid of metallic nanowires with diameter 100 nm as a function of wire spacing and THz wavelength, calculated using Equation (41). The contours are marked with the calculated values of $R_\parallel$ (b) polarization extinction ratio for a 5-μm spaced array of metallic nanowires as a function of nanowire diameter and wavelength of electromagnetic radiation, calculated using Equations (41) and (42). The contours are marked with the value of polarization extinction ratio in decibels (dB), i.e. 10 $\log_{10}(T_\perp/T_\parallel)$.

We now consider the reflection and transmission of a plane THz wave travelling in the + x-direction $E_0 e^{i(kx-\omega t)}$ at the grid of nanowires. For this case the solution of the wave equation in the region $x < 0$ includes the incident and reflected waves:

$$E(\mathbf{r},t) = \left[E_0 e^{ikx} + C_0 e^{-ikx} + \sum_{n=1}^{\infty} C_n e^{|k_n|x} \cos\frac{2\pi n y}{d}\right] e^{-i\omega t} \quad \text{for} \quad x < 0, \tag{37}$$

while for $x > 0$ only the transmitted wave is present,

$$E(\mathbf{r},t) = \left[D_0 e^{ikx} + \sum_{n=1}^{\infty} D_n e^{-|k_n|x} \cos\frac{2\pi n y}{d}\right] e^{-i\omega t} \quad \text{for} \quad x > 0. \tag{38}$$

Now assume that the wire separation is small compared with the wavelength of the THz light $d \ll \lambda$, therefore $(2\pi n/d)^2 \gg k^2$ so

$$|k_n| \approx \frac{2\pi n}{d} \quad (n > 0 \quad d \ll \lambda). \tag{39}$$

In addition, close to the wires x is small, so we may approximate $e^{ikx} \approx 1 + ikx$ giving the approximate solution close to the wires as

$$E(\mathbf{r},t) \approx \begin{cases} \left[E_0 + C_0 + ik(E_o - C_0)x + \sum_{n=1}^{\infty} C_n e^{2\pi n x/d} \cos\frac{2\pi n y}{d}\right] e^{-i\omega t} & \text{for} \quad x \lesssim 0 \\ \left[D_0(1+ikx) + \sum_{n=1}^{\infty} D_n e^{-2\pi n x/d} \cos\frac{2\pi n y}{d}\right] e^{-i\omega t} & \text{for} \quad x \gtrsim 0 \end{cases} \tag{40}$$

To find the Fourier coefficients $\{C_n\}$ and $\{D_n\}$ we need to consider the geometry of the nanowires and boundary conditions, i.e. from Maxwell's equations the tangential components of electric field must be zero at the nanowire surface and at $x = 0$, E and $\partial E/\partial x$ must be continuous.

4.1.1. *Case 1: Radiation polarized parallel to a wire grid polarizer*

We firstly consider the case of THz radiation with its electric field linearly polarized in the z-direction (i.e. parallel to the nanowire axes, $\hat{\mathbf{m}} = \hat{\mathbf{k}}$). In this case we note the $E = 0$ at the surfaces of the nanowires (as tangential component of electric field must be zero). For solutions of $E(\mathbf{r}, t)$ close to cylindrical wires (i.e. x and $(y - nd)$ small), the reflection and transmission coefficients may be approximated as [58],

$$R_\parallel = \left|\frac{C_0}{E_0}\right|^2 \approx \frac{1}{1 + C_\parallel^2 k^2 d^2}, \quad T_\parallel = \left|\frac{D_0}{E_0}\right|^2 \approx \frac{C_\parallel^2 k^2 d^2}{1 + C_\parallel^2 k^2 d^2}, \tag{41}$$

where we define $C_{\parallel} \equiv \frac{1}{2\pi}\ln[2 - 2\cos(2\pi a/d)]$. As we have assumed that $d \ll \lambda \equiv 2\pi/k$, then $C_{\parallel}kd$ is very small, for typical values of a/d. Therefore we expect near complete reflection of THz waves polarized parallel to the axes of the nanowires. However in the case that a/d is very small, $|C_{\parallel}|$ becomes large so the converse is true and the THz waves are nearly completely transmitted.

This allows us to examine the useful spectral range of nanowire wire grid polarizers. If we assume a grid of metallic nanowires with radius $a = 100$ nm and spacing $d = 5$ μm, then for THz radiation with wavelength 300 μm we expect 99.2% reflectivity, but for mid infrared light with wavelength 5 μm only 3.2% of the light is reflected. At visible wavelengths we expect nearly all the light to be transmitted (although our expressions derived here are no longer valid as we relied of the approximation $\lambda \gg d$). Fig. 7a shows reflectivity as a function of wavelength and nanowire spacing for 100 nm diameter nanowires.

4.1.2. Case 2: Radiation polarized perpendicular to a wire grid polarizer

In the case that the incident radiation is polarized perpendicular to the nanowire axis (i.e. electric field in the y-direction) then the reflection and transmission coefficients may be approximated as [58],

$$R_{\perp} = \left|\frac{D_0}{E_0}\right|^2 \approx \frac{C_{\perp}^2 k^2 d^2}{1 + C_{\perp}^2 k^2 d^2}, \quad T_{\perp} = \left|\frac{D_0}{E_0}\right|^2 \approx \frac{1}{1 + C_{\perp}^2 k^2 d^2} \tag{42}$$

where we define $C_{\perp} \equiv \frac{\cosh\frac{2\pi a}{d} - 1}{2\pi}$. In this case for a 5 μm-spaced grid of 100 nm-diameter nanowires we find that there is near 100% transmission of 300 μm THz radiation (only 1×10^{-7}% reflected)). While for 5μm mid-IR light 96.8% is transmitted.

So in this simple theoretical treatment the polarization extinction ratio $T_{\perp} : T_{\parallel}$ would be a reasonable 119:1 (or 21 dB) for 300 μm THz light, but a rather poor 1.03:1 (or 0.14 dB) for 5 μm mid IR light. Fig. 7b shows how the polarization extinction ratio (in dB) varies with wavelength and nanowire diameter for a grid of nanowires with a fixed spacing of 5 μm, according to our simple analytic treatment. It is clear that the extinction ratio increases sharply with both the wavelength of the THz radiation and nanowire diameter.

4.2. Experimental demonstration of nanowire-based THz polarization modulators

The principle described above was used to demonstrate a nanowire-based THz polarizer that could be switched on ultrashort timescales [11]. Arrays of highly aligned [111]B-oriented GaAs nanowires were grown via metalorganic chemical vapour deposition using the vapour–liquid–solid process with 50 nm-diameter Au nanoparticles as catalysts. The [111]B-oriented nanowires grew at angles of 35° to the substrate plane. When viewed as a projection onto the (100) plane, the nanowires appear parallel as in Fig. 6b, which is key to their role as a nanowire grid polarizer. The as-grown nanowires were embedded in Parylene-C polymer and this nanowire-in-polymer membrane was then removed from the growth substrate to create a substrate-free polarizer. Parylene-C was chosen as the host matrix because it is transparent at THz frequencies and at the 800 nm photoexcitation wavelength, mechanically robust and maintains the nanowires' highly parallel alignment. Layers of nanowires embedded in Parylene-C could were laminated together via a hot-bonding process to create multi-layer polarizers up to 14 layers thick. Each layer of nanowires-in-Parylene was approximately 5 μm thick, and the 14-layer polarizer was less than 100 μm thick. The photoconductivity response of these GaAs nanowires depends strongly on the polarization of the incident 800 nm beam, as was described in Section 2.1 and shown in Fig. 3b and c. Photoexcitation of the array with a pump pulse polarized parallel to the nanowires renders the nanowires conductive, which attenuates the transmission of the THz pulse, as illustrated in Fig. 8a–(i). On the other hand, excitation with a pulse polarized perpendicular to the nanowires causes little change in the nanowire conductivity, so that the THz pulse is minimally attenuated (Fig. 8a–(ii)). The modulation of THz transmission is plotted in Fig. 8b and follows the $\cos^2$ dependence on angle 2θ as predicted by Malus's law. Increasing the number of layers in the polarizer increases the effective density of GaAs nanowires, and therefore increases the modulation depth.

Narrow GaAs nanowires were chosen as the photoconductive constituents because they exhibit a rapid photoconductivity rise within less than 1 ps of photoexcitation at 800 nm, followed by a rapid photoconductivity decay of the order of a few picoseconds [51]. The rapid decay in photoconductivity is driven by non-radiative recombination at the nanowire surface [50]. This rapid modulation of conductivity gives rise to a rapid modulation of THz transmission, as plotted in Fig. 8c.

The demonstrated 14-layer polarizer featured a polarization extinction ratio of 1.01 dB, which is lower than suggested by the calculated data shown in Fig. 7, and indicates that increased control over NW orientation and position could vastly improve device performance. Nevertheless, these devices showed good modulation depth, broad bandwidth and picosecond switching speeds for THz intensity modulation, making them an ideal candidate for use as a modulator in ultrahigh speed THz communication systems.

5. Polarization-resolved THz detection using photoconductive nanowire antennas

In THz-TDS systems employing lasers with moderate pulse energies, photoconductive antennas (Auston switches) are the detectors of choice. The operating principle is that an above-bandgap photoexcitation pulse generates electrons and holes in the semiconductor, and the co-incident THz electric field drives these photogenerated electrons and holes towards the contacts. This THz-field induced photocurrent is measured and from it, the THz electric field can be inferred [59].

Single GaAs or InP nanowires are excellent candidates for the semiconductor material in THz photoconductive switches, as demonstrated by Peng et al. [60,61]. The nanowires employed within these devices exhibit relatively long charge carrier lifetimes ($>$ 100 ps) [22,62] and hence the resulting THz detectors operate in the integrating regime, whereby the measured photocurrent is

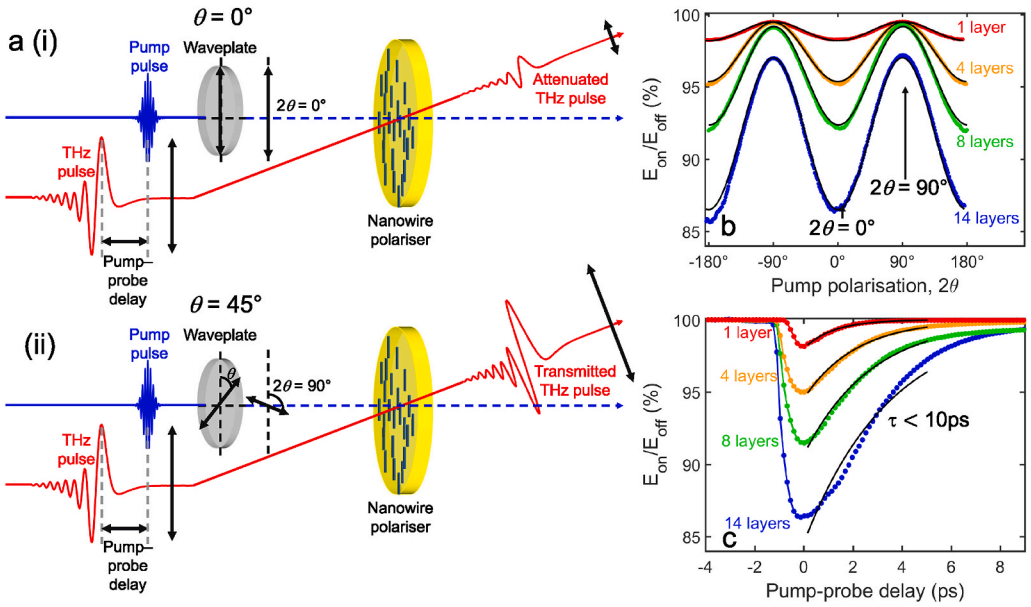

Fig. 8. (a) Diagram of the modulation scheme using zinc blende III–V nanowire grid polarizers. (i) Excitation with a laser polarized parallel to the nanowires causes attenuation of the transmitted THz pulse, whereas (ii) excitation polarized perpendicular to the nanowires has minimal effect. (b) Modulation of the transmitted THz pulse as a function of the polarization of the excitation laser relative to the nanowires, for multi-layer nanowire polarizers. (c) Modulation of the transmitted THz pulse as a function of time after photoexcitation with the excitation laser polarized parallel to the nanowire axis, for multi-layer nanowire polarizers. Modified and reproduced with permission from Baig et al. [11]. Copyright 2017 American Chemical Society.

proportional to the integrated THz electric field [59]. The demonstrated single-nanowire photoconductive THz detectors feature sub-wavelength size, making them suitable for near-field THz spectroscopy applications. Improvements were afforded by using bow-tie-shaped electrical contacts to enhance the antenna characteristics [61], and using highly n-doped regions at the nanowire ends to facilitate the formation of Ohmic contacts [63].

In general, the absorption of THz radiation by nanowires is highly dependent on polarization [51], with nanowires selectively absorbing THz electric field components parallel to the nanowire axis (as discussed in Section 3.2). In nanowire-based photoconductive detectors, this parallel component of the THz electric field causes current to flow along the nanowire axis. The magnitude of the current detected at the nanowire terminals is therefore sensitive to THz electric field parallel to the nanowire.

This principle was applied to devise a polarization-resolving photoconductive antenna based on orthogonally-crossed nanowires [34]. Fig. 9a and b show scanning electron micrographs of an example device, in which two pairs of nanowires are arranged orthogonal to one another in a hash(#)-like geometry. This spatial arrangement was achieved by sequentially transfer-printing [64] individual InP nanowires. Orthogonal nanowires are electrically isolated from one another, whereas parallel wires have common electrodes. Thus, sets of orthogonally-oriented nanowires can detect both THz electric field components simultaneously. The data in Fig. 9c were simultaneously acquired from the horizontal channel (horizontal nanowires) and the vertical channel (vertical nanowires) of the detector. The horizontally-oriented nanowires selectively detected the horizontal components of the THz electric field, whereas the vertically-oriented nanowires selectively detected the vertical component. The bow-tie antennas formed by the contacts are also strongly polarization sensitive, and selectively concentrate electric field components parallel to the nanowire axis onto the nanowire to enhance the overall polarization sensitivity of the detector.

The nanowire hash detector successfully resolved both polarizations with minimal cross-talk (Fig. 9d) or shadowing, which was only possible because of the unique anisotropic optical and geometrical properties of semiconductor nanowires. Already these nanowire detectors have accurately discriminated the polarization of incident THz pulses (Fig. 9e) and observed the manipulation of THz polarization in sub-wavelength patterned metamaterials [34]. Furthermore they are well suited to applications in polarization-resolved spectroscopy including birefringence, optical activity and circular dichroism [25] as well as time-resolved cyclotron resonance [32]. The detector concept also has great potential for extending THz polarimetry into imaging applications such as polarization-enhanced THz imaging [65] and THz nanoscopy [66].

6. Conclusion

Semiconductor and metallic nanowires feature marked optical anisotropy which can be exploited in polarization-sensitive opto-electronic devices. Nanowire-based polarization devices operating in the THz band, such as THz polarization modulators and THz polarimetric detectors, have been demonstrated and are anticipated to enable new applications in THz sensing, imaging, non-

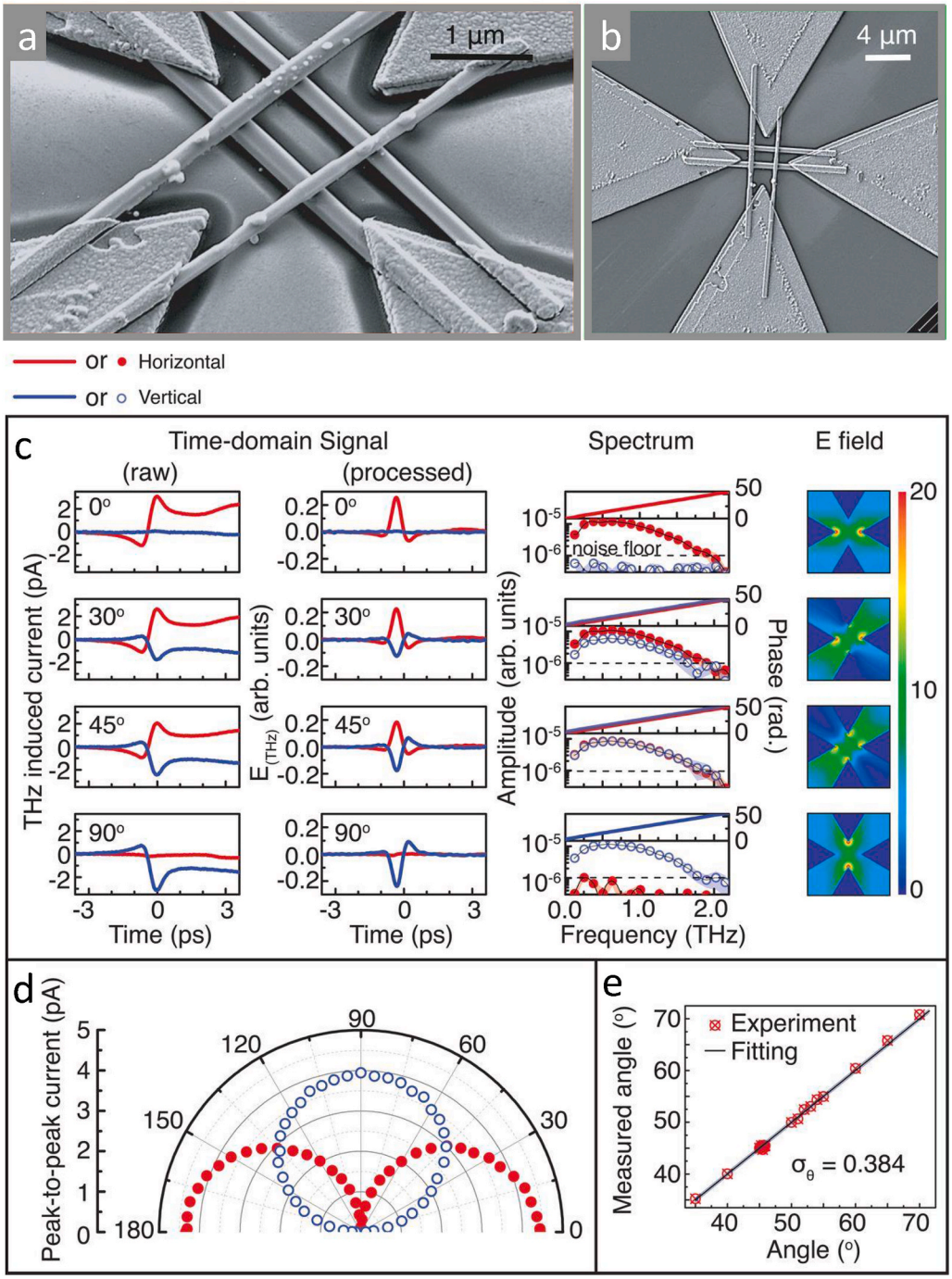

Fig. 9. Scanning electron micrographs of the polarization-sensitive cross-nanowire THz detector showing (a) higher magnification image of the nanowire morphology and arrangement and (b) lower magnification image of the nanowires with bow-tie antenna-shaped electrical contacts. (c) The measured current, the extracted THz time-domain signal, the extracted THz spectra and the simulated electric field for various polarizations (0°, 30°,45°, and 90°) of incident THz radiation. (d) Polar plot of the peak THz-induced current in the horizontal and vertical nanowires. (e) THz polarization angle measured using the detector, versus rotation angle of the THz emitter. Modified and reproduced with permission from Peng et al. [34].

destructive testing and communications. Although this review has primarily focussed on the THz band, the polarization anisotropy inherent to nanowires can be exploited in devices operating in other parts of the electromagnetic spectrum [13,14]. Combining polarization sensitivity with other unique nanowire features, such as optical memory effects [67] could also provide novel device

functionality. Nanowire-based polarimetric devices and polarization-modulating devices based on nanowires will underpin new optoelectronic systems in the THz band and beyond.

Acknowledgements

M.B.J. gratefully acknowledges the support of the EPSRC-UK (grant EP/T025077/1). H.J.J. gratefully acknowledges support from the European Research Council (ERC Starting Grant no. 716471, ACrossWire).

References

[1] J. Wang, M.S. Gudiksen, X. Duan, Y. Cui, C.M. Lieber, Highly polarized photoluminescence and photodetection from single indium phosphide nanowires, Science 293 (2001) 1455–1457.
[2] H.E. Ruda, A. Shik, Polarization-sensitive optical phenomena in semiconducting and metallic nanowires, Phys. Rev. B 72 (2005), 115308.
[3] H.E. Ruda, A. Shik, Polarization-sensitive optical phenomena in thick semiconducting nanowires, J. Appl. Phys. 100 (2006), 024314.
[4] L.V. Titova, T.B. Hoang, H.E. Jackson, L.M. Smith, J.M. Yarrison-Rice, Y. Kim, H.J. Joyce, H.H. Tan, C. Jagadish, Temperature dependence of photoluminescence from single core-shell GaAs–AlGaAs nanowires, Appl. Phys. Lett. 89 (2006), 173126.
[5] T.B. Hoang, L.V. Titova, J.M. Yarrison-Rice, H.E. Jackson, A.O. Govorov, Y. Kim, H.J. Joyce, H.H. Tan, C. Jagadish, L.M. Smith, Resonant excitation and imaging of nonequilibrium exciton spins in single core–shell GaAs–AlGaAs nanowires, Nano Lett. 7 (2007) 588–595.
[6] J.L. Birman, Polarization of fluorescence in CdS and ZnS single crystals, Phys. Rev. Lett. 2 (1959) 157–159.
[7] J.L. Birman, Some selection rules for band-band transitions in wurtzite structure, Phys. Rev. 114 (1959) 1490–1492.
[8] A. Mishra, L.V. Titova, T.B. Hoang, H.E. Jackson, L.M. Smith, J.M. Yarrison-Rice, Y. Kim, H.J. Joyce, Q. Gao, H.H. Tan, C. Jagadish, Polarization and temperature dependence of photoluminescence from zincblende and wurtzite InP nanowires, Appl. Phys. Lett. 91 (2007), 263104.
[9] P.C. Sercel, K.J. Vahala, Analytical technique for determining the polarization dependence of optical matrix elements in quantum wires with band-coupling effects, Appl. Phys. Lett. 57 (1990) 545–547.
[10] C.R. McIntyre, L.J. Sham, Theory of luminescence polarization anisotropy in quantum wires, Phys. Rev. B 45 (1992) 9443–9446.
[11] S.A. Baig, J.L. Boland, D.A. Damry, H.H. Tan, C. Jagadish, H.J. Joyce, M.B. Johnston, An ultrafast switchable terahertz polarization modulator based on III–V semiconductor nanowires, Nano Lett. 17 (2017) 2603–2610.
[12] S. Pournia, S. Linser, G. Jnawali, H.E. Jackson, L.M. Smith, A. Ameruddin, P. Caroff, J. Wong-Leung, H.H. Tan, C. Jagadish, H.J. Joyce, Exploring the band structure of wurtzite inas nanowires using photocurrent spectroscopy, Nano Res. 13 (2020) 1586–1591.
[13] S. Deshpande, J. Heo, A. Das, P. Bhattacharya, Electrically driven polarized single-photon emission from an InGaN quantum dot in a GaN nanowire, Nat. Commun. 4 (2013) 1675.
[14] R.T. Velpula, B. Jain, M.R. Philip, H.D. Nguyen, R. Wang, H.P.T. Nguyen, Epitaxial growth and characterization of AlInN-based core-shell nanowire light emitting diodes operating in the ultraviolet spectrum, Sci. Rep. 10 (2020) 2547.
[15] M. Möller, M.M. de Lima, A. Cantarero, L.C.O. Dacal, J.R. Madureira, F. Iikawa, T. Chiaramonte, M.A. Cotta, Polarized and resonant Raman spectroscopy on single InAs nanowires, Phys. Rev. B 84 (2011), 085318.
[16] B. Ketterer, M. Heiss, E. Uccelli, J. Arbiol, A. Fontcuberta i Morral, Untangling the electronic band structure of wurtzite GaAs nanowires by resonant Raman spectroscopy, ACS Nano 5 (2011) 7585–7592.
[17] W. Peng, F. Jabeen, B. Jusserand, J.C. Harmand, M. Bernard, Conduction band structure in wurtzite GaAs nanowires: a resonant Raman scattering study, Appl. Phys. Lett. 100 (2012), 073102.
[18] P. Kusch, S. Breuer, M. Ramsteiner, L. Geelhaar, H. Riechert, S. Reich, Band gap of wurtzite GaAs: a resonant Raman study, Phys. Rev. B 86 (2012), 075317.
[19] C. Fasolato, I. Zardo, M. De Luca, in: N. Fukata, R. Rurali (Eds.), Fundamental Properties of Semiconductor Nanowires, Springer, Singapore, 2021, pp. 307–348. Ch. Addressing Crystal Structure in Semiconductor Nanowires by Polarized Raman Spectroscopy.
[20] B. Mirkhaydarov, H. Votsi, A. Sahu, P. Caroff, P.R. Young, V. Stolojan, S.G. King, C.C.H. Ng, V. Devabhaktuni, H.H. Tan, C. Jagadish, P.H. Aaen, M. Shkunov, Solution-processed InAs nanowire transistors as microwave switches, Adv. Electron. Mater. 5 (2019), 1800323.
[21] P.J. Reece, S. Paiman, O. Abdul-Nabi, Q. Gao, M. Gal, H.H. Tan, C. Jagadish, Combined optical trapping and microphotoluminescence of single InP nanowires, Appl. Phys. Lett. 95 (2009), 101109.
[22] H.J. Joyce, Q. Gao, H. Hoe Tan, C. Jagadish, Y. Kim, J. Zou, L.M. Smith, H.E. Jackson, J.M. Yarrison-Rice, P. Parkinson, M.B. Johnston, III–V semiconductor nanowires for optoelectronic device applications, Prog. Quant. Electron. 35 (2011) 23–75.
[23] K. Peng, M.B. Johnston, The application of one-dimensional nanostructures in terahertz frequency devices, Appl. Phys. Rev. 8 (2021), 041314.
[24] S.S. Dhillon, M.S. Vitiello, E.H. Linfield, A.G. Davies, M.C. Hoffmann, J. Booske, C. Paoloni, M. Gensch, P. Weightman, G.P. Williams, E. Castro-Camus, D.R. S. Cumming, F. Simoens, I. Escorcia-Carranza, J. Grant, S. Lucyszyn, M. Kuwata-Gonokami, K. Konishi, M. Koch, C.A. Schmuttenmaer, T.L. Cocker, R. Huber, A. G. Markelz, Z.D. Taylor, V.P. Wallace, J.A. Zeitler, J. Sibik, T.M. Korter, B. Ellison, S. Rea, P. Goldsmith, K.B. Cooper, R. Appleby, D. Pardo, P.G. Huggard, V. Krozer, H. Shams, M. Fice, C. Renaud, A. Seeds, A. Stöhr, M. Naftaly, N. Ridler, R. Clarke, J.E. Cunningham, M.B. Johnston, The 2017 terahertz science and technology roadmap, J. Phys. D Appl. Phys. 50 (2017), 043001.
[25] E. Castro-Camus, M.B. Johnston, Extraction of the anisotropic dielectric properties of materials from polarization-resolved terahertz time-domain spectra, J. Opt. Pure Appl. Opt. 11 (2009), 105206.
[26] J. Federici, L. Moeller, Review of terahertz and subterahertz wireless communications, J. Appl. Phys. 107 (2010) 111101.
[27] T. Kürner, D.M. Mittleman, T. Nagatsuma, THz Communications: Paving the Way Towards Wireless Tbps, Springer, Cham, 2021.
[28] M. Okano, S. Watanabe, Anisotropic optical response of optically opaque elastomers with conductive fillers as revealed by terahertz polarization spectroscopy, Sci. Rep. 6 (2016), 39079.
[29] D.M. Mittleman, J. Cunningham, M.C. Nuss, M. Geva, Noncontact semiconductor wafer characterization with the terahertz Hall effect, Appl. Phys. Lett. 71 (1997) 16–18.
[30] T. Matsuda, N. Kanda, T. Higo, N.P. Armitage, S. Nakatsuji, R. Matsunaga, Room-temperature terahertz anomalous Hall effect in Weyl antiferromagnet Mn_3Sn thin films, Nat. Commun. 11 (2020) 909.
[31] M. Neshat, N.P. Armitage, Terahertz time-domain spectroscopic ellipsometry: instrumentation and calibration, Opt Express 20 (2012) 29063–29075.
[32] C.Q. Xia, M. Monti, J.L. Boland, L.M. Herz, J. Lloyd-hughes, M.R. Filip, M.B. Johnston, Hot electron cooling in InSb probed by ultrafast time-resolved terahertz cyclotron resonance, Phys. Rev. B 103 (2021), 245205.
[33] N. Yasumatsu, S. Watanabe, T-ray topography by time-domain polarimetry, Opt. Lett. 37 (2012) 2706–2708.
[34] K. Peng, D. Jevtics, F. Zhang, S. Sterzl, D.A. Damry, M.U. Rothmann, B. Guilhabert, M.J. Strain, H.H. Tan, L.M. Herz, L. Fu, M.D. Dawson, A. Hurtado, C. Jagadish, M.B. Johnston, Three-dimensional cross-nanowire networks recover full terahertz state, Science 368 (2020) 510–513.
[35] F. Vouilloz, D.Y. Oberli, M.-A. Dupertuis, A. Gustafsson, F. Reinhardt, E. Kapon, Effect of lateral confinement on valence-band mixing and polarization anisotropy in quantum wires, Phys. Rev. B 57 (1998) 12378–12387.
[36] M. Tsuchiya, J.M. Gaines, R.H. Yan, R.J. Simes, P.O. Holtz, L.A. Coldren, P.M. Petroff, Optical anisotropy in a quantum-well-wire array with two-dimensional quantum confinement, Phys. Rev. Lett. 62 (1989) 466–469.
[37] E.A. Muljarov, E.A. Zhukov, V.S. Dneprovskii, Y. Masumoto, Dielectrically enhanced excitons in semiconductor-insulator quantum wires: theory and experiment, Phys. Rev. B 62 (2000) 7420–7432.

[38] C. Wilhelm, A. Larrue, X. Dai, D. Migas, C. Soci, Anisotropic photonic properties of III–V nanowires in the zinc-blende and wurtzite phase, Nanoscale 4 (2012) 1446–1454.
[39] H.J. Joyce, J. Wong-Leung, Q. Gao, H.H. Tan, C. Jagadish, Phase perfection in zinc blende and wurtzite III–V nanowires using basic growth parameters, Nano Lett. 10 (2010) 908–915.
[40] A. De, C.E. Pryor, Predicted band structures of III–V semiconductors in the wurtzite phase, Phys. Rev. B 81 (2010), 155210.
[41] L. Ahtapodov, J. Todorovic, P. Olk, T. Mjåland, P. Slåttnes, D.L. Dheeraj, A.T.J. van Helvoort, B.-O. Fimland, H. Weman, A story told by a single nanowire: optical properties of wurtzite GaAs, Nano Lett. 12 (2012) 6090–6095.
[42] S. Perera, T. Shi, M.A. Fickenscher, H.E. Jackson, L.M. Smith, J.M. Yarrison-Rice, S. Paiman, Q. Gao, H.H. Tan, C. Jagadish, Illuminating the second conduction band and spin–orbit energy in single wurtzite inp nanowires, Nano Lett. 13 (2013) 5367–5372.
[43] K. Seo, M. Wober, P. Steinvurzel, E. Schonbrun, Y. Dan, T. Ellenbogen, K.B. Crozier, Multicolored vertical silicon nanowires, Nano Lett. 11 (2011) 1851–1856.
[44] H.-S. Ee, K.-D. Song, S.-K. Kim, H.-G. Park, Finite-difference time-domain algorithm for quantifying light absorption in silicon nanowires, Isr. J. Chem. 52 (2012) 1027–1036.
[45] E.A. Dawi, A.A. Karar, E. Mustafa, O. Nur, Plasmon-enhanced light absorption in (p-i-n) junction GaAs nanowire solar cells: an FDTD simulation method study, Nanoscale Res. Lett. 16 (1) (2012) 1027–1036.
[46] Z. Zhang, Z. Zhang, L. Zhang, C. Huang, Z. Xiong, Electric field enhancements around the nanorod on the base layer, Opt Express 19 (2011) 7274–7279.
[47] D. Whittaker, I. Culshaw, Scattering-matrix treatment of patterned multilayer photonic structures, Phys. Rev. B 60 (1999) 2610–2618.
[48] L. Ren, C.L. Pint, T. Arikawa, K. Takeya, I. Kawayama, M. Tonouchi, R.H. Hauge, J. Kono, Broadband terahertz polarizers with ideal performance based on aligned carbon nanotube stacks, Nano Lett. 12 (2012) 787–790.
[49] C.J. Docherty, S.D. Stranks, S.N. Habisreutinger, H.J. Joyce, L.M. Herz, R.J. Nicholas, M.B. Johnston, An ultrafast carbon nanotube terahertz polarisation modulator, J. Appl. Phys. 115 (2014), 203108.
[50] H.J. Joyce, C.J. Docherty, Q. Gao, H.H. Tan, C. Jagadish, J. Lloyd-Hughes, L.M. Herz, M.B. Johnston, Electronic properties of GaAs, InAs and InP nanowires studied by terahertz spectroscopy, Nanotechnology 24 (2013), 214006.
[51] H.J. Joyce, S.A. Baig, P. Parkinson, C.L. Davies, J.L. Boland, H.H. Tan, C. Jagadish, L.M. Herz, M.B. Johnston, The influence of surfaces on the transient terahertz conductivity and electron mobility of GaAs nanowires, J. Phys. D Appl. Phys. 50 (2017), 224001.
[52] G.R. Bird, M. Parrish, The wire grid as a near-infrared polarizer, J. Opt. Soc. Am. 50 (1960) 886–891.
[53] F. Yan, C. Yu, H. Park, E.P.J. Parrott, E. Pickwell-MacPherson, Advances in polarizer technology for terahertz frequency applications, J. Infrared, Millim. Terahertz Waves 34 (2013) 489–499.
[54] Rayleigh, On the dynamical theory of gratings, Proc R. Soc. Lond. A Math. Phys. Sci 79 (1907) 399–416.
[55] Rayleigh, On the passage of waves through apertures in plane screens, and allied problems, Phil. Mag. 43 (1897) 259–272.
[56] J.J. Thompson, Recent Researches in Electricity and Magnetism, Clarendon Press, Oxford, 1893.
[57] H. Lamb, On the reflection and transmission of electric waves by a metallic grating, Proc. Lond. Math. Soc. 29 (1898) 523.
[58] K.T. McDonald, Wire polarizers. https://www.hep.princeton.edu/ mcdonald/examples/polarizer.pdf, 2012. (Accessed 10 March 2022).
[59] E. Castro-Camus, L. Fu, J. Lloyd-Hughes, H.H. Tan, C. Jagadish, M.B. Johnston, Photoconductive response correction for detectors of terahertz radiation, J. Appl. Phys. 104 (2008), 053113.
[60] K. Peng, P. Parkinson, L. Fu, Q. Gao, N. Jiang, Y.-N. Guo, F. Wang, H.J. Joyce, J.L. Boland, H.H. Tan, C. Jagadish, M.B. Johnston, Single nanowire photoconductive terahertz detectors, Nano Lett. 15 (2015) 206–210.
[61] K. Peng, P. Parkinson, J.L. Boland, Q. Gao, Y.C. Wenas, C.L. Davies, Z. Li, L. Fu, M.B. Johnston, H.H. Tan, C. Jagadish, Broadband phase-sensitive single InP nanowire photoconductive terahertz detectors, Nano Lett. 16 (2016) 4925–4931.
[62] H.J. Joyce, P. Parkinson, N. Jiang, C.J. Docherty, Q. Gao, H.H. Tan, C. Jagadish, L.M. Herz, M.B. Johnston, Electron mobilities approaching bulk limits in "surface-free" GaAs nanowires, Nano Lett. 14 (2014) 5989–5994.
[63] K. Peng, P. Parkinson, Q. Gao, J.L. Boland, Z. Li, F. Wang, S. Mokkapati, L. Fu, M.B. Johnston, H.H. Tan, C. Jagadish, Single n^+-i-n^+ InP nanowires for highly sensitive terahertz detection, Nanotechnology 28 (2017), 125202.
[64] B. Guilhabert, A. Hurtado, D. Jevtics, Q. Gao, H.H. Tan, C. Jagadish, M.D. Dawson, Transfer printing of semiconductor nanowires with lasing emission for controllable nanophotonic device fabrication, ACS Nano 10 (2016) 3951–3958.
[65] S. Watanabe, Terahertz polarization imaging and its applications, Photonics 5 (2018) 58.
[66] T. Siday, F. Sandner, S. Brem, M. Zizlsperger, R. Perea-Causin, F. Schiegl, S. Nerreter, M. Plankl, P. Merkl, F. Mooshammer, M.A. Huber, E. Malic, R. Huber, Ultrafast nanoscopy of high-density exciton phases in WSe_2, Nano Lett. 22 (2022) 2561–2568.
[67] J.A. Alexander-Webber, C.K. Groschner, A.A. Sagade, G. Tainter, M.F. Gonzalez-Zalba, R. Di Pietro, J. Wong-Leung, H.H. Tan, C. Jagadish, S. Hofmann, H. J. Joyce, Engineering the photoresponse of InAs nanowires, ACS Appl. Mater. Interfaces 9 (2017) 43993–44000.